Effects of Grain and Aft-Dome Configuration on Aft-End SRB Internal Flows

R. H. W. Waesche*
Atlantic Research Corporation, Gainesville, Virginia 22065
and
J. F. Marchman† and S. Kuppa‡
Virginia Polytechnic Institute and State University, Blacksburg, Virginia 24061

A series of cold-flow tests was conducted to determine the effects of configuration on the aft-end internal flowfield of candidate Space Shuttle boosters. Initially, the effects of Reynolds number were studied in an extension of earlier water flow-visualization tests in a ⅛-scale model of the High-Performance Motor (HPM). No significant change in the nozzle-inlet vortex formation previously reported was noted at higher Reynolds number. Changes in aft-dome contour, submerged-nozzle contour, and aft-segment grain design were then evaluated in the water tunnel to aid in the selection of a candidate grain and dome for the Advanced Solid Rocket Motor (ASRM). Models representing the grain at ignition and at 35 s into the firing were fabricated and changes in the flow patterns documented. Using a tapered-grain model with the HPM nozzle/aft dome produced more intense vortex formation and circumferential flows than when a nontapered-grain configuration was employed. Significant changes were observed when the first ASRM nozzle/aft dome was installed with the tapered grain; no circumferential flow was observed when the nozzle was in the unvectored position. In addition, dye placed in the base of the aft dome cleared this region more rapidly than for any other configuration tested. Tests with the redesigned ASRM nozzle/aft dome and aft-slot grain design indicated that this redesigned aft dome led to reduced circumferential flows. The effects of nozzle vectoring on flow character were far less marked with this configuration than for the HPM. These models were then tested in a series of cold-gas tests. Pressure, velocity, and turbulence intensity were mapped near the nozzle entrance plane and in the aft dome. The results of the cold-gas tests showed the same effects of grain/dome configuration as did the observations made in the water-flow tests.

Introduction

As part of a program to develop an Advanced Solid Rocket Motor (ASRM) for the Space Shuttle, testing was conducted, employing ⅛-scale model tests in air and/or water, to examine the internal flows in the aft portion of candidate ASRM designs. These tests were conducted in the water-tunnel facility described in Ref. 1 and in an airflow facility constructed specifically for these tests.

Water-tunnel tests were conducted with the High-Performance Motor (HPM) nozzle/aft-dome design tested in Ref. 1, both with a tapered-grain model representing the configuration 60 s into a firing and with an untapered-grain model. This testing was conducted at higher mass flows and, hence, Reynolds numbers higher than those used in earlier tests.[1] In addition, water-tunnel testing was conducted of the preliminary ASRM nozzle/aft-dome design with the tapered grain, then of candidate ASRM aft-fin grain designs and aft-dome designs. Tests were run for configurations representing the grain at ignition and at 35 s into the firing. These tests were qualitative in nature, employing flow visualization to evaluate these candidate designs and to assist in final configuration selection.

Received May 9, 1989; presented as Paper 89-2421 at the AIAA 25th Joint Propulsion Conference, Monterey, CA, July 10-13, 1989; revision received and accepted for publication May 25, 1990.

*Principal Scientist, Virginia Propulsion Division, 5945 Wellington Rd. Fellow AIAA.

†Associate Dean for Academic Affairs, School of Engineering. Associate Fellow AIAA.

‡Research Assistant; currently with Analytical Services and Materials, Inc., 107 Research Dr., Hampton, VA 23666.

The objectives of the tests done under this part of the program were as follows:

1) Examine the effects of flow Reynolds number in water-tunnel testing of HPM flows.

2) Compare the results of tests with a tapered-grain model with those of earlier tests with an untapered model.

3) Test a preliminary candidate ASRM nozzle/aft-dome design with the tapered-grain model.

4) Test this nozzle/aft-dome with a model based on the preliminary ASRM grain design.

5) Test the final ASRM nozzle/aft-dome and grain design.

Since the present tests did not require characterizing the flows in the SRM joint regions, the models tested could be greatly simplified relative to those tested earlier.[1] Figure 1 shows the model of the aft segment of the HPM (including dome and nozzle) in the water-tunnel test section. A detailed view of one of the models tested (the preliminary ASRM nozzle/aft-dome design with tapered 60-s grain) is shown in Fig. 2. The secondary flow plenum was greatly simplified when compared with the one employed in Ref. 1. Four separate secondary flow lines were mated with the upstream portion of the grain model, and a regulated flow was pumped by the secondary pumps into the region between the model wall and the grain surface model. The downstream half of the grain was perforated with nearly 1000 ¼-in. holes to allow simulation of the grain surface mass flow as flow was pumped through the secondary system. Once again, careful balancing of the main and secondary flow rates was used to match properly the core/aft-segment-grain mass-flow ratio in the actual HPM.

Flow visualization was achieved by the use of fluoroscein dye, a water-soluble dye that fluoresces at a characteristic light frequency. High-intensity photofloodlights were used to illuminate the dye flow patterns. All flow tests were recorded on standard VHS videotape using a Panasonic Reporter, Professional Model Camcorder.

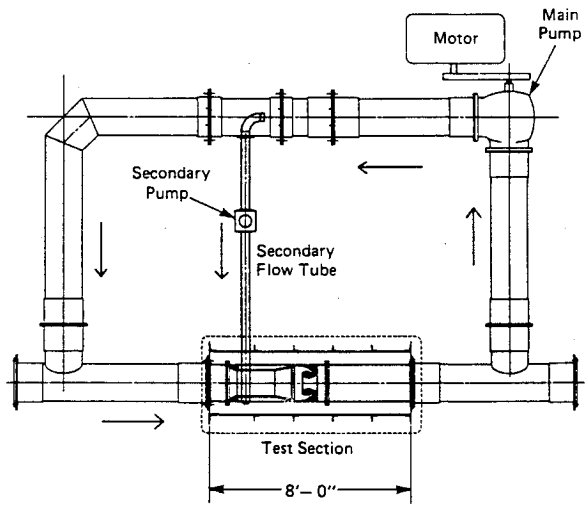

Fig. 1 Modified water tunnel.

Earlier tests[1] of SRM internal flows conducted in the Virginia Polytechnic Institute water tunnel showed significant circumferential and vortical flow patterns within a ⅛-scale of the high-performance Morton-Thiokol (HPM) design for the Space Shuttle SRM. The validity of these results had been questioned because of the test Reynolds numbers and because of the use of a straight-grain model instead of a model that would simulate more accurately the grain configuration existing at 60-s burning time in the aft segment of the HPM.

Although previous tests[2-6] in water-flow simulations of the internal flow in combustors have all confirmed that the overall character of the flow remains unchanged for test Reynolds numbers from 10^4 to 10^7, questions have arisen from researchers as to the validity of rocket-motor simulation over a range of Reynolds numbers. To answer such questions, the initial portion of water-tunnel testing was devoted to retesting the HPM nozzle/aft dome with the 60-s grain model at higher internal-flow speeds (and, hence, higher *Re*) than were used in the previous tests, which were conducted at $Re > 7 \times 10^4$. This testing was made possible by a redesign of the water tunnel and the purchase of a higher power pump motor and an improved control system for the tunnel.

The airflow tests comprised cold-flow testing in an airflow facility to document pressure and velocity profiles in the model representing the chosen ASRM configuration. These cold-air procedures were then repeated for the HPM aft dome and tapered grain.

The several combinations of grain and dome/nozzles tested are summarized in Table 1.

Facility

Water-Tunnel Redesign

Two factors limited the model core flow rate with the Ref. 1 water tunnel as it was configured for the earlier HPM internal-flow tests. First, the motor and its control system were limited in their output. Second, the restrictor plate used to force flow into the secondary flow plenum limited the flow through the remainder of the system.

For the present tests, the water tunnel was reconfigured as shown in Fig. 1. A new variable-speed motor and motor control were used to drive the main system pump, allowing higher flow rates. The restrictor plate/secondary plenum system was replaced with a simple out-take line and a secondary flow pump. This secondary pump was also a variable-speed pump with a variable-frequency-control system. This new configuration allowed independent regulation of the main and secondary flow rates without restricting the main flow. Through this system, core flow Reynolds numbers close to 5×10^5 could easily be achieved, as compared with 4×10^7 in Ref. 1. The only limit on flow velocity was that imposed by cavitation in the test-nozzle throat.

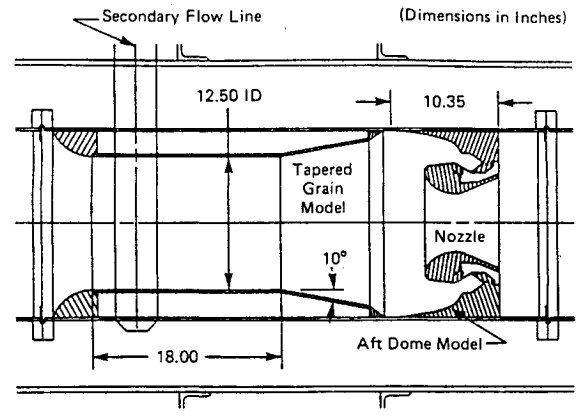

Fig. 2 Tapered-grain model with preliminary nozzle and aft-dome design.

Table 1 Test matrix

Grain[a]	Dome/nozzle	Test medium
HPM 60 s	ASRM I[b]	Water
HPM 60 s	HPM	Water, air
ASRM I zero time	ASRM I	Water
ASRM I 35 s	ASRM I	Water
ASRM F[b] zero time	ASRM F	Water, air
ASRM F 35 s	ASRM F	Water, air

[a]The grain tested represents the configuration that would exist at the burning time shown.
[b]ASRM I—preliminary ASRM design; ASRM F—final ASRM design.

Cold-Air Test System

The final ASRM model and the HPM model were also tested in a cold-air test system. To conduct the cold-air tests, a special facility was constructed using a high-capacity industrial centrifugal blower to pull air through the ⅛-scale model. Figure 3 shows the ASRM ignition-time model mounted to the blower via a diffuser. Flow entered the system through the bell-mouth sections shown, entering the core flow either directly via the center pipe or via the slots and holes in the finned-grain model. Extensive measurements and several preliminary test runs were conducted to set the ratio of core-to-fin mass flow rate required to match that predicted from ballistic predictions for the ASRM design. The mass flow through the model and, hence, velocity were limited by the capacity of the blower and the pressure drop across the model. All tests reported next were conducted at maximum blower velocity, which led to a Reynolds number of 4×10^5 at the aft end of the grain portion of the model, close to the Reynolds number in the water-flow tests. The aft-dome portion of the model was equipped with 48 pressure taps, as shown in Figs. 4 and 5. These pressure taps were connected to a single pressure sensor via a computer-driven scanning system.

The pressure distributions in the aft dome were tabulated in the form of pressure coefficients C_p relative to conditions at the upstream end of the grain segment:

$$C_p = (p_{\text{loc}} - p_{\text{ups}}) / \tfrac{1}{2} \rho_{\text{ups}} V^2_{\text{ups}}$$

Although absolute values cannot be compared with operational conditions, relative values are still indicative of those expected.

Hot-wire anemometer measurements were also used to determine velocity profiles. Figure 6 shows the hot-wire anemometer traverse location, and Fig. 7 shows the two hot-wire alignments employed. When the wire is aligned in the θ-Z plane, it measures a combination of tangential and axial flow.

When it is aligned in the r-θ plane, it responds to a combination of radial and axial flow. A more complete separation of the components of the flow requires a multicomponent probe of the type designed by Dunlap et al.[7]

Test Results

Water Tunnel

Reynolds Number Effects

The first tests were conducted using the HPM nozzle/aft-dome design shown in Fig. 8. To determine the potential effects of increased flow speed, i.e., Reynolds number, on the flow patterns previously reported,[1] tests were conducted at Reynolds numbers up to 10 times those reported in Ref. 1, with no changes in the general character of the flow observed. The primary flow patterns of interest observed were still circumferential flows in the nozzle/aft-dome region both due to vectoring of the nozzle and to inlet vortices between the HPM outer wall and the nozzle inlet. The inlet vortices were accentuated by vectoring. The only effect noted due to increasing the *Re* of the core flow was an increase in the aft-dome local flow velocities which appeared to match the increase in core flow speed, implying that there would be Reynolds numbers effects on the magnitude of velocities in the dome.

These tests confirmed the results reported in Ref. 1 and the concept of a critical *Re* required for effective water testing, as reported in Refs. 2–6. These results were shown quite clearly on videotape made during the tests.

Tapered-Grain Effects

The second series of tests conducted in the water tunnel employed the HPM nozzle/aft dome; however, a tapered-grain model was used to simulate the grain surface. Figure 8 compares the straight-grain 60-s model used both in the Ref. 1 study and in the tests reported earlier with the actual HPM 60-s grain. Figure 2 shows the tapered-grain model constructed for these tests (shown with the ASRM nozzle/aft dome). This tapered-grain model was scaled from the HPM

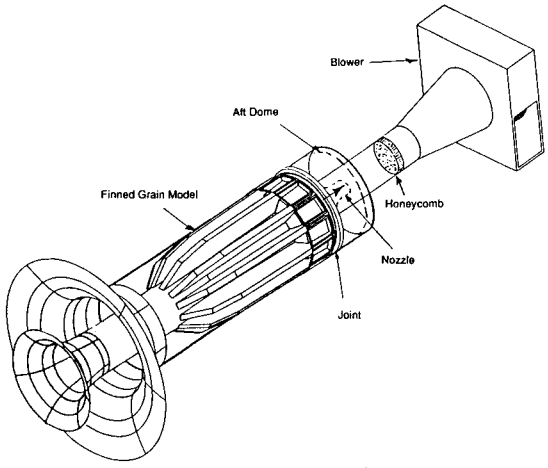

Fig. 3 Cold-air test system.

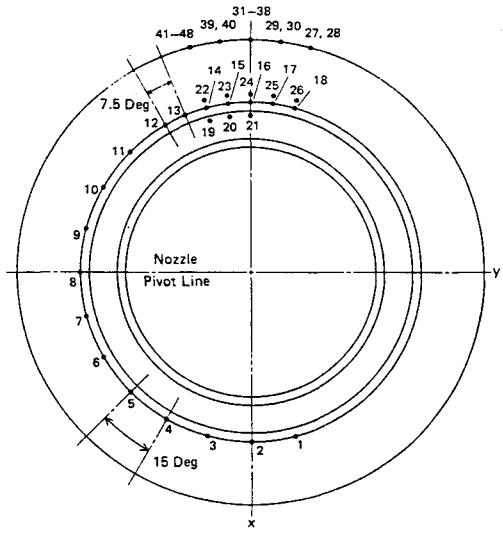

Fig. 4 Pressure tap distribution (end view).

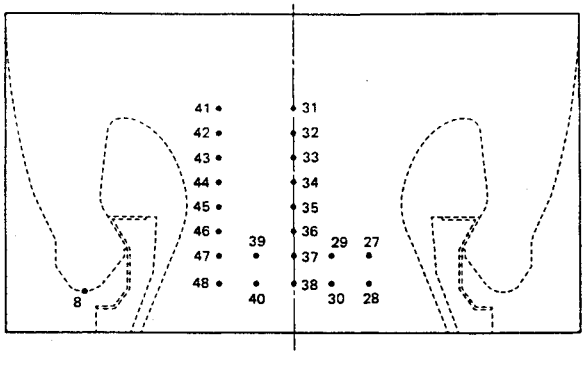

Side View

Fig. 5 Pressure tap distribution (side view).

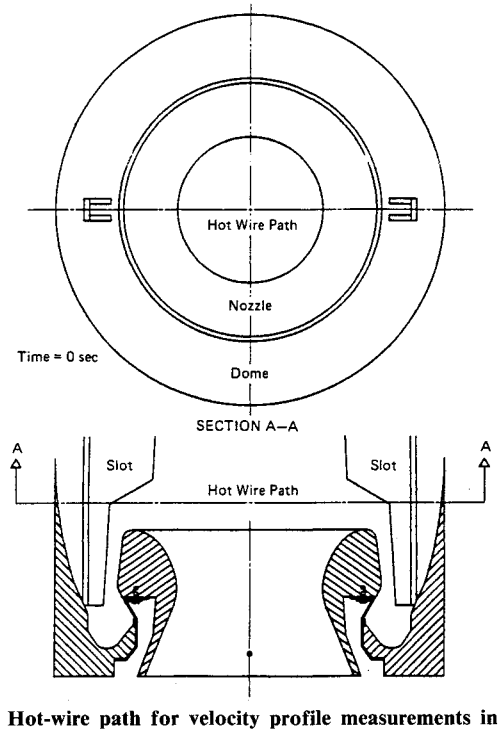

Fig. 6 Hot-wire path for velocity profile measurements in ASRM model.

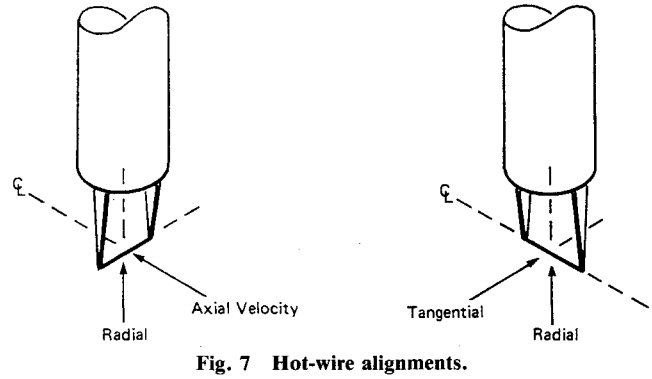

Fig. 7 Hot-wire alignments.

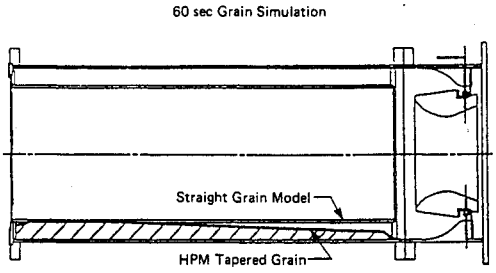

Fig. 8 Comparison of actual and model aft segment grains with HPM nozzle and aft segment grains with HPM nozzle and aft-dome design.

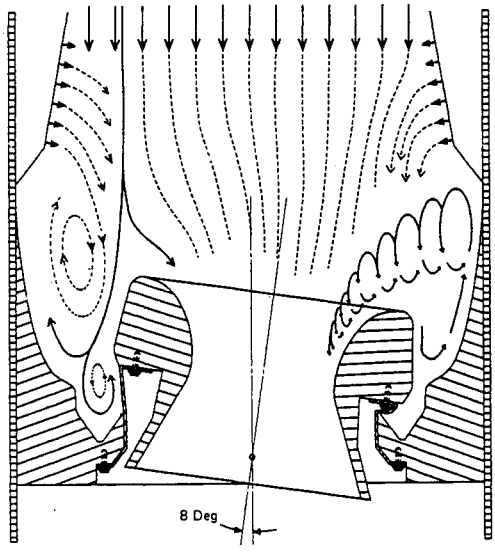

Fig. 9 Flow in model with HPM tapered grain.

60-s grain pattern and was used to evaluate the effects of the tapered grain on the previously observed flow patterns.

Tests using the tapered 60-s grain model with the HPM nozzle/aft dome displayed more intense vortex formation and circumferential flow than were seen in the tests with the nontapered grain model. Multiple vortices were clearly seen forming between the outer wall and the nozzle entrance at virtually any nozzle vector angle. Another pronounced result of the change to a tapered-grain model was the tendency of the vortex to go further upstream of the nozzle entrance than in the previous case. When the nozzle was vectored, dye injected into the aft-dome area often moved well upstream of the nozzle entrance before being entrained into the core flow. There was also a significant increase in circulatory flow in the aft dome when the nozzle was vectored, with dye often traveling over 180 deg before ingestion into the nozzle.

Nozzle/Dome Effects

The next tests employed the tapered-grain model and the preliminary ASRM nozzle/aft-dome design. This is the configuration shown in Fig. 2. Significant differences were seen between these test results and those using the same grain model with the HPM nozzle/aft dome. Dye injected into the aft-dome region moved upstream, out of the dome region, before experiencing any significant circumferential flow. A representative flow pattern is sketched in Fig. 9. For the flow pattern sketched in this figure, the nozzle is vectored 8 deg to illustrate the effects of maximum deflection. In this configuration, dye injected into any area upstream of the nozzle entrance moves generally into the core flow and into the nozzle. Dye injected into the region surrounding the forward portion of the nozzle moves upstream and then into the core flow, experiencing a circumferential flow as it moves upstream. None

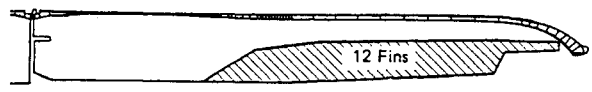

Fig. 10 ASRM aft-slot design.

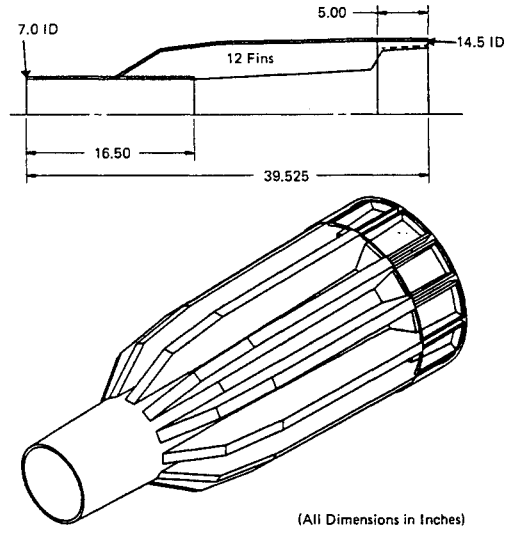

Fig. 11 ASRM aft-fin grain model.

of the dye injected into this region tended to move aft into the small volume at the base of the aft dome. Dye injected into the base of the aft dome was rapidly pumped out and upstream toward the core flow.

No circumferential flow was noted when the nozzle was in the unvectored position of the preliminary ASRM nozzle/aft-dome design when employed with the tapered HPM grain. This lack of circumferential flow was not true for any other configuration tested.

Preliminary Advanced Solid Rocket Motor Grain Design

The first series of tests were run using a preliminary ASRM nozzle/aft-dome configuration with the preliminary aft-finned grain shown in Figs. 10 and 11. Not shown in Fig. 11 are the more than 6000 holes drilled in the grain model, through which secondary flow was pumped to simulate grain mass flow. To achieve more uniform injection and to attempt to simulate the radial momentum of the injected fluid, shown to be significant in Refs. 8 and 9, the holes near the aft end of the slot were ⅛ in. in diameter, rather than the ¼-in. holes further upstream, near the minimum practical size allowing for visualization. The secondary-flow/core-flow mass-flow ratio was set to duplicate the 41/59 mass-flow ratio of the ASRM design at the initiation of burning. The preliminary grain design—an attempt to maximize propellant loading and thereby to achieve greater payload—was mated with the preliminary nozzle/aft-dome model and tested in the water tunnel to examine the flow patterns in the nozzle/aft-dome region resulting from the maximized loading.

Figure 12 shows a sketch of the flow patterns for the preliminary grain with the vectored nozzle. It was seen that dye injected into the base of the aft dome below the downward-vectored nozzle did not move upstream because of the restricted area available for flow, but remained in the base of the aft dome for an extended period as it moved circumferentially around the aft dome until there was sufficient grain-nozzle clearance to allow its escape. This often required a circumferential motion of 130–140 deg.

Flow visualization also showed that dye injected into the slots between the fins in the region around the nozzle usually

moved rapidly upstream into the core flow and into the nozzle. When the nozzle was close to the fins, as in the vectored-nozzle case, dye injected into the aft region of the slot was trapped in the aft-dome base area until it flowed around the nozzle base to an escape zone. When the nozzle was not vectored, there was less entrapment of this base area flow. The flow moving upstream from the grain surrounding the nozzle mixed with the flow from the slot areas upstream of the nozzle to obscure any jetting effects from the slots, and all flow appeared to move readily into the nozzle.

Tests were also conducted, at a range of nozzle vector angles, with a model of the preliminary candidate grain design's surface 35 s into the burn. This time is approximately the point at which the grain has burned away sufficiently for the base of the slots to have reached the wall. The absence of grain around the nozzle at this time allows normal free flow around the nozzle/aft-dome region. The unique flow characteristics noted in videotapes of these tests were the strong tendency for backflow from the aft-dome region and the circumferential flows induced by apparent vortex shedding from the fin remnants in the grain.

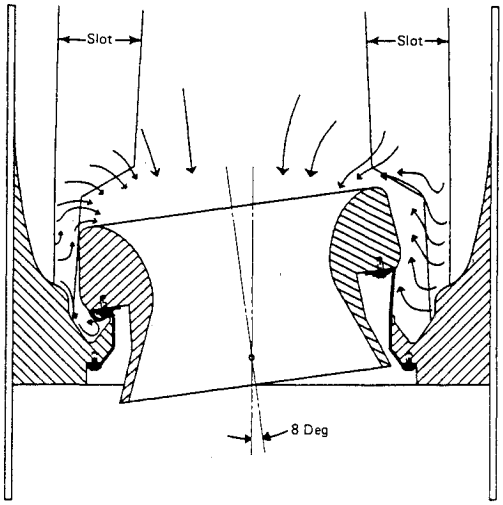

Fig. 12 Flow in preliminary ASRM design (nozzle vectored 8 deg).

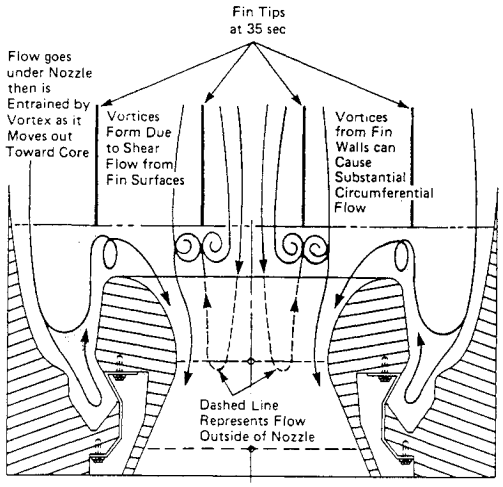

Note: Flows Shown are Near Wall Flows only
Core Flow goes Directly into Nozzle

Fig. 13 Sketch of flows for preliminary ASRM design at 35 s.

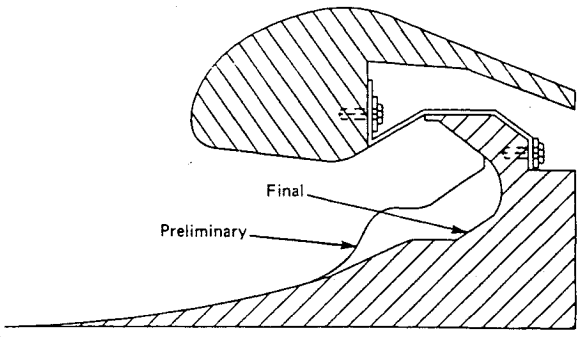

Fig. 14 Preliminary and final ASRM aft-dome contours.

Vortices shed from the remnants of the fins of the downstream grain lead to alternating vortex motions and radial vortices between the ends of the fins and the core flow. This vortex flow appears to pump flow upstream from the aft-dome region and then to impart circumferential motion to the flow when it reaches the fin-termination region, after which it enters the core flow and the nozzle. This flow is best seen in the videotapes from these tests; an attempt is made to sketch the flow in Fig. 13.

Final Advanced Solid Rocket Motor Grain and Dome

As a result of these tests, both the candidate ASRM aft-segment grain design and aft-dome contour were modified. The grain was modified in the nozzle region to allow better nozzle clearance at ignition and the aft dome was reshaped with thinner insulation. The reduction in insulation thickness was based on the development of material that was more resistant to erosion, thereby allowing more propellant to be cast in that area. The aft-dome model was therefore remachined to the new contour as shown in Fig. 14, and the grain model was modified to duplicate the design changes.

These modifications altered the flow patterns noted with the preliminary ASRM aft-dome design with the finned grain. Flow from the rearmost part of the grain (at the base of the aft dome) tended to remain in that region for an extended time. Vectoring of the nozzle to the full extent caused circumferential flow; this flow had lower apparent velocities than those observed earlier for the HPM design. The majority of the aft-fin segment flow moved upstream into the core flow and into the nozzle, as illustrated in Fig. 15. Flow from the upstream slot areas mixed with the flow from around the nozzle via vortices shed from the fins, then spread circumferentially in both directions to mix with flow from the adjacent slot before entering the nozzle.

Two important features are to be noted from these flow observations. First, the aft-dome flowfield following burnout of propellant in the dome is more stagnant in nature than that for the HPM, implying less convective heat transfer. Second, the circumferential flows are characterized by lower velocity, implying a decreased tendency for erosion of material from both the nozzle and the insulation.

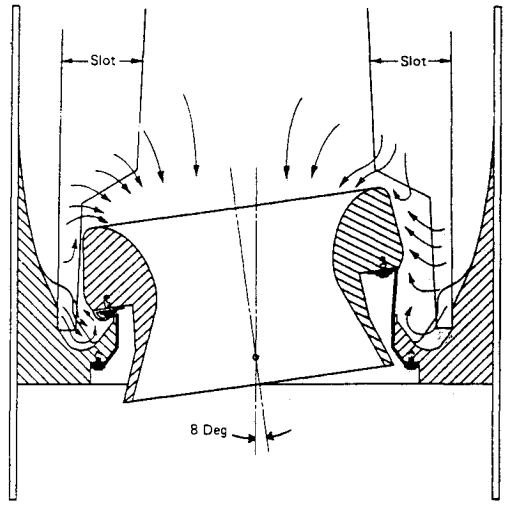

Fig. 15 Ignition-time flow in final ASRM design.

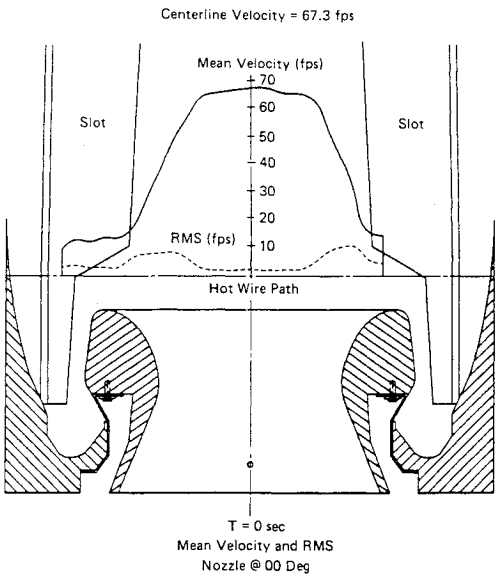

Fig. 16 Velocity profiles—ASRM model ($t = 0$, 0-deg vector).

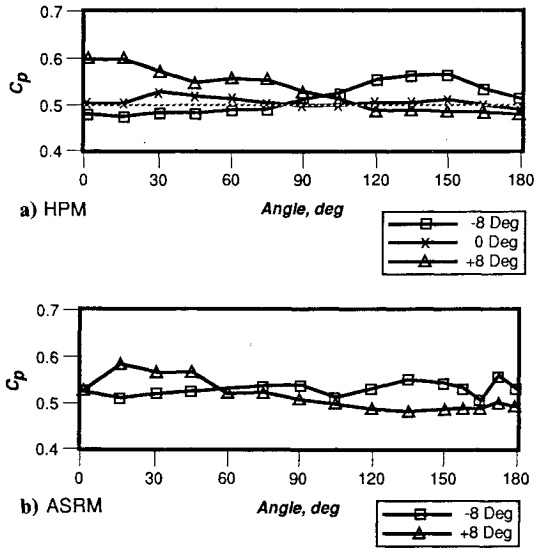

Fig. 17 Effect of nozzle vector on aft-dome C_p distribution: a) HPM; b) ASRM.

Cold-Air Flow Tests

As mentioned earlier, cold-air flow tests were conducted to map the velocity and pressure distributions in the aft end of the final ASRM design and the HPM.

Advanced Solid Rocket Motor Model

Hot-wire anemometry was used to measure velocity profiles at the ASRM fin-pattern break point, i.e., at the axial location where the fin opened to the wall, in front of the nozzle at several nozzle vector angles. Typical data are shown in Fig. 16. Also shown to scale on the figure are the rms velocities or turbulence levels. The turbulence levels are highest just outside of the slots. The results of a traverse with the hot wire aligned parallel to the system axis show that the "transverse" (combination of radial and tangential) velocities are small compared with the centerline velocity.

The variation in values of pressure coefficient C_p and in the character of the distribution of pressures is small from one nozzle vector angle to another, from 5 to 10% as the nozzle was vectored (Fig. 17a). The magnitude of pressure coefficient values did increase as the nozzle vector angle was increased. These data indicate, as did the water-flow tests, that flow in the region is not driven by large transverse pressure gradients.

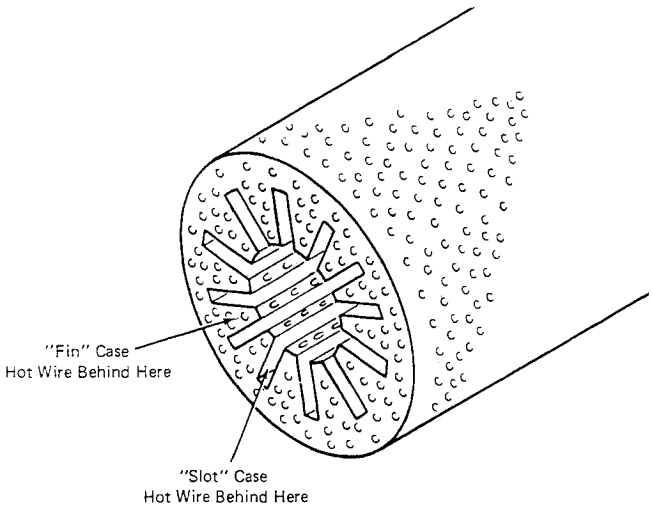

Fig. 18 Hot-wire location.

The data also indicate that the effects of the aft-slot grain design on the aft-dome insulation are minimal, i.e., no pattern corresponding to the slots is observed. The distributions measured in the aft-dome base above the nozzle also show that the pressure increases as the nozzle is vectored toward the taps and decreases when vectored away from the taps. Again, however, the changes in the magnitude of local pressure are small.

The next model tested was the 35-s finned grain. Again the same model was used as was tested in water, and tests were run to set the proper mass-flow ratio between the core flow and the fins. The same pressure tap arrangement described in Figs. 12 and 13 was used.

The velocity and turbulence level data (in a plane a short distance upstream of the nozzle) for the case where the nozzle was not vectored indicate a fully developed core flow with a small radial component as the flow moves toward the nozzle. There is an increase in the nonaxial velocity components as the nozzle entrance is vectored. The rms data indicate that the tangential component is greatest at the sector of the nozzle on the side with the greatest flow area, whereas the radial component of velocity is probably most pronounced in front of the nozzle on the opposite side.

Measurements were also made by placing the hot-wire probe into the region of the aft dome between the outer nozzle wall and the dome wall with the probe support parallel to the system axis. The probe could be moved forward from the base of the aft dome toward the upstream fins. Once again, the probe was used with two wire orientations, one where the wire was aligned with a system radial line and the other with the wire perpendicular to the radial (Fig. 7). One orientation allows measurement of a combination of tangential and axial flows; the other, a combination of radial and axial flows.

Data were taken for both a "fin" and a "slot" case. These refer to tests where the hot-wire anemometer was placed downstream of and in line with a fin or a slot in the grain, respectively (Fig. 18). As expected, the measurements made behind a slot result in slightly higher nonaxial components of the velocity, and the axial velocities decrease as the base of the aft dome is approached while the tangential/radial component first decreases, then increases as the base of the dome is approached. Plots of all data can be found in Ref. 10.

The overall pressure pattern indicates a relatively stagnant area around the nozzle and in the aft dome for the 35-s case. This generally agrees with the flow-visualization results, which show the flow in this region to be circling in and back out into the core area.

High-Performance Motor Model

To complete comparison between the HPM and ASRM, the tapered-grain model with the HPM nozzle/dome assembly

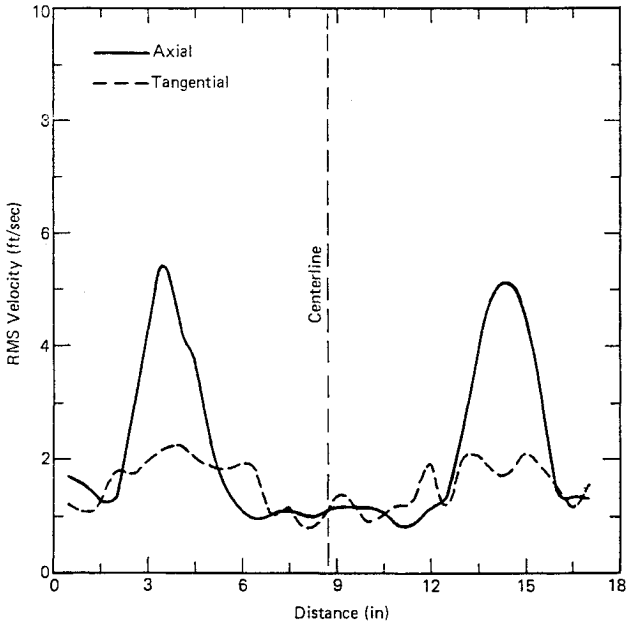

Fig. 19 Velocity profile for HPM nozzle (unvectored).

was tested in air. The model was assembled as in Fig. 11 and connected to the suction side of the blower, as was done for the air tests of the ASRM models. Enough holes were made in the outer 18-in. pipe to obtain the required ratio between the core flow and the flow through the holes in the grain model. For these tests, the pressure taps were located as for the ASRM tests. Velocity profiles were also mapped with the use of a hot-wire anemometer just in front of the nozzle and also under the nozzle in the area between the nozzle and aft dome. The nozzle was vectored at -8, -4, 0, $+4$, and $+8$ deg while making pressure and velocity measurements under the nozzle. In addition, the nozzle was vectored at -8, -4, and 0 deg while making the velocity measurements in front of the nozzle. Velocity measurements between the outer nozzle wall and the dome wall were made in the same way as for the ASRM tests. Once again, details of the data are given in Ref. 10. They indicate that, where the nozzle is unvectored, there is a well-developed symmetric core flow with a small radial component (Fig. 19). Measurements of velocity made between the outer nozzle wall and the dome wall indicated that the flow is essentially stagnant in this region.

Pressure data for the HPM model were obtained for pressure tap distributions comparable to those for the ASRM model. The values of the pressure coefficient are about the same in magnitude as in the 35-s case for the ASRM. However, unlike the results for the ASRM tests, these figures show variations in the pressure distribution as the nozzle is vectored from -8 to $+8$ deg (Fig. 17b). The pressure distribution shows a gradient of nearly 25% for the vectored nozzle and essentially none for the unvectored case. Furthermore, the change in the pressure pattern is symmetric with the change in the nozzle vector angle, thus showing that the model and the flow were symmetrical. The circumferential pressure gradient indicates the presence of a circumferential flow when the nozzle is vectored. The values of C_p and the gradient obtained from the two concentric rows of pressure taps agree very well with each other.

A review of the pressure distribution parallel to the axis of the model indicates a gradient toward upstream when the nozzle is vectored away from the dome wall, whereas when the nozzle is vectored toward the dome wall, the gradient disappears. This is due to the slight increase or decrease in velocities around the nozzle as the vectoring increases or decreases the volume available to the flow in that region.

Summary and Conclusions

A number of important conclusions can be drawn from this series of cold-flow tests. First, the finding that overall flow characteristics were insensitive to an order-of-magnitude change in Reynolds number, once the flow was fully turbulent, reinforces the findings of other researchers and further corroborates the Ref. 1 characterization of the aft-dome flowfield of the HPM. Second, the finding that the use of a tapered-grain model intensified vortex formation activity indicates that changes in grain geometry and, as a result, changes in the flow profile, can effect changes in the aft-dome cavity flowfield. This means that accurate grain simulation is an important consideration in developing a true picture of internal-flow structure. Third, the correlation between the flow-visualization observations made in water and the flowfield measurements made in air further reinforces the value of the flow-visualization technique.

Other conclusions relate to the candidate aft-slot ASRM configuration. Both the flow-visualization observations and the pressure-distribution measurements of Fig. 17 indicate that the aft-dome cavity is relatively stagnant, especially as compared with that for the HPM. This finding implies that design of thermal protection for the aft dome and the outer surface of the submerged nozzle can be simplified. Furthermore, the hot-wire data do not indicate severe gradients in turbulence in the aft-slot region. There are random circumferential flows and vortex shedding off the fins at the face of the nozzle. These flows help to pump the flow forward from the grain-slot areas in the aft dome and to impart a random circumferential component of the flow entering the nozzle. Vectoring of the nozzle had only a very small influence on the aft-dome pressure distribution and flow pattern.

The water-flow tests with the HPM nozzle/aft dome and a tapered aft grain segment indicated that intense vortical flow was observed when the nozzle was vectored, whereas tests in air with the HPM geometry revealed that the circumferential pressure distribution on the aft dome was quite sensitive to changes in the nozzle vector angle, reinforcing these visual observations.

These cold-flow techniques represent valuable tools for further design trade studies. In addition, the detailed velocity and pressure measurements can be employed to provide a data base with which computational fluid dynamic codes can be calibrated, since the properties of the gas are well known. It is possible to investigate changes in slot width, boattails, etc., with changes in model components.

Acknowledgments

The assistance provided by W. Cowardin in fabricating the complex models required for these tests cannot be recognized adequately. In addition, C. Hetreed and P. Keitel assisted in recording data and in providing the computer-aided design representations and data plots. They performed invaluable roles. This work was performed under Hercules-Atlantic funding.

References

[1]Waesche, W., Sargent, W. H., and Marchman, J. F., "Space Shuttle Solid Rocket Motor Aft-End Internal Flows," *Journal of Propulsion and Power*, Vol. 5, No. 6, 1989, pp. 650–656.

[2]Winter, E. F., "Flow Visualization Techniques Applied to Combustion Problems," *Journal of the Royal Aeronautical Society*, Vol. 62, April 1958, pp. 268–276.

[3]Winter, E. F., and Deterding, J. H., "Apparatus and Techniques for the Application of a Water Flow System to the Study of Aerodynamic Systems," *British Journal of Applied Physics*, Vol. 7, 1956, pp. 247–260.

[4]Clarke, A. E., Gerrard, A. J., and Holliday, L. A., "Some Experiences in Gas Turbine Combustion Chamber Practice Using Water Flow Visualization Techniques," *Ninth Symposium (International) on Combustion*, Reinhold, 1962, pp. 878–891.

[5]Kennedy, J. B., "Ramburner Flow Visualization Studies," Chemical Propulsion Information Agency, Pub. 261, Sept. 1974, pp. 415–440.

[6]Schetz, J. A., Hewitt, P. A., and Thomas, R., "Swirl Combustor Flow Visualization Studies in a Water Tunnel," *Journal of Spacecraft and Rockets*, Vol. 20, No. 6, 1983, pp. 574–582.

[7]Dunlap, R. A., Blackner, A. M., Waugh, R. C., Brown, R. S., and Willoughby, P. G., "Internal Flow Field Studies in a Simulated Cylindrical Port Rocket Chamber," *Journal of Propulsion and Power*, Vol. 6, No. 6, 1990, pp. 690–704.

[8]Dunlap, R., Willoughby, P. G., and Hermsen, R. W., "Flowfield in the Combustion Chamber of a Solid Propellant Rocket Motor," *AIAA Journal*, Vol. 12, No. 10, 1974, pp. 1440–1442.

[9]Taylor, G. I., "Fluid Flow in Regions Bounded by Porous Surfaces," *Proceedings of the Royal Society of London, Series A: Mathematical and Physical Sciences*, Vol. 234, 1956, pp. 456–475.

[10]Hetreed, C. F., "Internal Flow Investigation of an Aft Finocyl Grain Configuration in a Solid Rocket Motor," M. S. Thesis, Virginia Polytechnic Institute and State University, Blacksburg, VA, July 1989.